The Effect of Cold Climate upon North Atlantic Deep Water Formation in a Simple Ocean–Atmosphere Model

MICHAEL WINTON

Geophysical Fluid Dynamics Laboratory/NOAA, Princeton University, Princeton, New Jersey

(Manuscript received 29 December 1995, in final form 16 April 1995)

ABSTRACT

The sensitivity of North Atlantic Deep Water formation to variations in mean surface temperature is explored with a meridional-vertical plane ocean model coupled to an energy balance atmosphere. It is found that North Atlantic Deep Water formation is favored by a warm climate, while cold climates are more likely to produce Southern Ocean deep water or deep-decoupling oscillations (when the Southern sinking region is halocline covered). This behavior is traced to a cooling-induced convective instability near the North Atlantic sinking region, that is, to unstable horizontal spreading of a halocline that stratifies part of the region. Under the convective instability it is found that climate cooling is generally equivalent to increased freshwater forcing. This is because in a cold climate, high-latitude water masses approach the temperature of maximum density and the convection-driving, upward thermal buoyancy flux induced by surface cooling becomes insufficient to overcome the stratifying effect of surface freshening (a downward buoyancy flux). An extensive halocline is then formed and this halocline interferes with the heat loss necessary for the steady production of North Atlantic Deep Water.

1. Introduction

The polar ice and ocean sediment cores reveal a glacial climate that was very different from that of the Holocene—both in its mean and in its variability. The changes seem to have been particularly pronounced in the subpolar North Atlantic Ocean and adjacent land regions. This is a part of the globe that is significantly influenced by the formation of North Atlantic Deep Water (NADW) in today's climate. Variations in NADW formation are implicated, more or less directly, in many of the changes seen in the paleo-record. Results from mixed-boundary condition ocean-only models and fully coupled climate models have indicated that the thermohaline processes involved in formation of NADW make it susceptible to changes in the environment and, under some circumstances, internal variations. This paper is directed toward understanding these processes in more detail and demonstrating how they might help to understand the record. This is a speculative venture—and it will be useful to approach it armed with two paradigms for thermohaline circulation instability distilled from idealized models. After a review of relevant aspects of the paleo-record in section two, these simple models are described in section three. In particular, it will be shown that one of the two kinds of instability, convective instability, is potentially affected by climate cooling. To investigate this possibility in more detail a coupled ocean–atmosphere model is developed in section three. The model is used in section four to examine the steady or statistically stationary response of NADW formation to surface climates with a range of mean temperatures. The results are discussed in section five.

2. The paleo-record

The most direct evidence for glacial era changes in NADW formation comes from from the nutrient proxies Cd/Ca and ^{13}C incorporated in shells of benthic foraminifera. These show that the low nutrient signal of the NADW diminished during the cold Younger Dryas period (Boyle and Keigwin 1987) and that during the last glacial maximum, a nutrient depleted intermediate water was formed instead (Duplessy et al. 1988).

The Greenland ice core ^{18}O records show that the cold climate of the last ice age was punctuated with occasional warm (''interstadial'') periods lasting from several hundred to several thousand years (Dansgaard et al. 1993). The transitions between the warm and cold periods were abrupt—the most recent warmings following the last glacial and Younger Dryas cold periods took place in just 50 years (Alley et al. 1993). These Dansgaard–Oeschger (D–O) events have been well correlated with foraminiferal indicators of sea surface temperatures (SSTs) buried in the North Atlantic ocean sediments (Bond et al. 1993). The global nature of the events is revealed by their methane signal (Chappellaz et al. 1993) also present in the Greenland ice cores, and the

Corresponding author address: Dr. Michael Winton, GFDL/NOAA, Princeton University, P.O. Box 308, Princeton, NJ 08542.
E-mail: mw@gfdl.gov

presence of muted features corresponding to many of the events in the Vostok Antarctic ice core (Dansgaard et al. 1993). Recently, the foram record has been extended back to the Eemian interglacial period (McManus et al. 1994; Keigwin et al. 1994). While confirming the D–O events during the glacial times, unstable North Atlantic SSTs were not detected in the last warm period corresponding to today's climate.

The Greenland ice sheet is ideally situated to record variations in the formation of North Atlantic Deep Water that occur in the adjacent Greenland, Norwegian, and Labrador Seas. A plausible hypothesis for the temperature signal recorded by the ice cores is that it reflects the magnitude of oceanic heat loss associated with the formation of this water mass.

The NADW hypothesis is attractive because numerous modeling results show that the opposition of thermal and haline forcing involved in NADW formation is capable of producing multiple equilibria and internal variability. The most complete of these studies was performed by Manabe and Stouffer (1988). They showed that a coupled ocean–atmosphere model has two stable equilibria: one with and one without NADW formation. The difference in the two climates was most pronounced in the North Atlantic region where warmer sea surface and surface air temperatures and reduced sea ice accompany NADW production. Manabe and Stouffer showed further that the freshening of the North Atlantic in the NADW off mode is due to the increased water residence time in the region of freshening rather than changes in the hydrological cycle—in other words, it is due to internal ocean processes rather than a coupled ocean–atmosphere interaction. If we accept that these two climate modes underlie the paleo-record, we are faced with two questions. 1) Why has the deep circulation of the Atlantic been locked in the NADW forming mode since the end of the Younger Dryas, about 11 000 years ago? And 2) how do transitions between the two modes occur?

The most obvious place to look for answers to these questions is in the freshwater flux into the North Atlantic. During glacial times, ice sheets greatly enhanced the freshwater storage capacity of the land as well as the potential for pulselike release. There is evidence for such impulsive freshwater inputs, but it is hard to reconcile with direct forcing of mode switches. First consider the period of deglaciation that began 14 000 years ago. The sea level record from the Barbados corals shows that the warm periods before and after the Younger Dryas contained meltwater spikes with melting rates near 0.4 Sv (Fairbanks 1989). The melting was considerably reduced during the cold Younger Dryas period. This suggests a negative feedback: reduced ocean heat transport leads to reduced melting allowing increased overturning. Impulsive freshwater inputs also occur during the heart of the glacial period. Recently, layers of ice-rafted debris associated with enormous calving events of the Laurentide ice sheet have been discovered in the subpolar North Atlantic (see review in Broecker 1994). These ''Heinrich events'' are typically spaced at 10 000-yr intervals and occur during the cold part of the D–O cycles. The volume of ice involved in these discharges has been estimated to be nearly one-half of the current Greenland ice sheet or 5% of the Laurentide ice sheet at its maximum (MacAyeal 1993). MacAyeal estimates the associated freshwater flux at 0.16 Sv (1 Sv $\equiv 10^6$ m^3 s^{-1}, about one-half of the current net freshening of the subpolar North Atlantic). The Heinrich events occur within the D–O cold phases and precede warm phases, sometimes by a substantial interval. The H1 event, for example, preceded the warming at 12 700 ^{14}C years BP by some 1400 years. Thus, these large impulsive salinity forcings are not easily connected to apparent changes in NADW production. A further difficulty concerns the average behavior of NADW in glacial and interglacial times. Since the hydrological cycle is expected to be stronger in warm climates, we would expect there to be on average *more* NADW production in the cold glacial climates rather than less, even if there were greater intermittancy due to variability in the land-based freshwater stock.

A more promising correlation seemingly exists between cooling and thermohaline circulation mode than between freshwater forcing and thermohaline circulation mode. The warm climate of the Holocene has been accompanied by steady NADW production, and there is some evidence that this was also true of the last (Eemian) interglacial. The intervening glacial period contains a long era of persistent instability as well as apparently steady North Atlantic Intermediate Water formation at the last glacial maximum. Atmospheric models have shown that the ice sheets exert a powerful cooling influence upon the subpolar North Atlantic (Kutzbach and Wright 1985; Manabe and Broccoli 1985). Anticyclonic low-level winds over the ice sheets funnel Arctic air into this region. The strength of this circulation has been reported to be sensitive to the size of the ice sheet (Kutzbach and Ruddiman 1993).

Bond et al. (1993) have noted that the D–O events are grouped into long-term cooling cycles bracketed by Heinrich events. The interstadials decrease in duration with cooling in these ''Bond cycles.'' The interstadials are also longer in the warmer, earlier part of the glacial-interglacial cycle (isotope stage 5) than in the colder, later stages. This and the apparent reduction of NADW formation during the coldest part of the glacial, the last glacial maximum, suggest a correlation between reduced NADW formation and cooling within the glacial period, as well as throughout the entire cycle.

3. Advective and convective instabilities

To highlight some of the important considerations involved in thermohaline circulation stability, we will consider the response to strong steady freshwater forcing of two Cartesian coordinate models. Both models

are based upon a meridional momentum balance between the pressure gradient force and a Rayleigh friction acting upon the meridional velocity:

$$rv = \frac{-1}{\rho_0}\frac{\partial P}{\partial y}, \tag{1}$$

and use the linear equation of state:

$$\rho(T, S) = S - T, \tag{2}$$

where ρ is density, T is temperature, and S is salinity. The first model is perhaps the simplest such model of the conflict between thermal and haline forcing for control of the buoyant overturning: the Stommel two-box model (Stommel 1961; Marotzke 1989). Here we use a variant of this model that, after nondimensionalizing, has two free parameters: F, the magnitude of the salt flux from the high-latitude box to the low-latitude box, and P, a coefficient for restoring the thermal difference between the boxes to a reference value. This model is identical to that of Marotzke except that we allow the temperature difference to deviate from its reference value. The equations for the differences in salinity, ΔS, and temperature, ΔT, between the low- and high-latitude boxes are

$$\frac{\partial \Delta S}{\partial t} = -2|\Delta T - \Delta S|\Delta S + 2F \tag{3}$$

$$\frac{\partial \Delta T}{\partial t} = -2|\Delta T - \Delta S|\Delta T + P(1 - \Delta T). \tag{4}$$

The second model is a continuous, two-dimensional, meridional-vertical plane model based upon the model of Winton (1995b) but extended to include salinity. This model is distinguished from the first by its ability to represent stratification effects including the nonlinear dependence of vertical mixing upon stratification (convective adjustment). The uppermost model grid layer is forced by restoring temperatures to a half-cosine-shaped reference profile with a restoring parameter, P, and applying half-cosine-shaped salt fluxes with a magnitude, F.

We shall compare these two models in terms of the *critical level of freshening* or F_{crit}. This is defined to be the level of freshening at which a steady thermally direct (cold-water sinking) circulation becomes untenable. The supercritical behavior may be oscillatory or a steady haline-direct circulation, depending upon the model. The critical levels of the two models are plotted as a function of thermal restoring strength, P, in Fig. 1 (thick dashed lines).

Figure 1a also shows contours of the two-box model overturning magnitude, $\Delta T - \Delta S$, nomalized by its value with the same restoring, P, but no freshwater forcing ($F = 0$) in the region of the parameter space with a stable, thermally dominated steady state. Two aspects of the two box model plot are noteworthy: 1) with stronger thermal restoring, more freshening can be sustained by a thermally direct flow; 2) a substantial reduction of the overturning (more than 40%) occurs before the thermally dominated solution becomes untenable. Both of these properties are evidence of an *advective* instability: The salinity gradient retards the overturning, increasing the influence of the salinity flux boundary condition

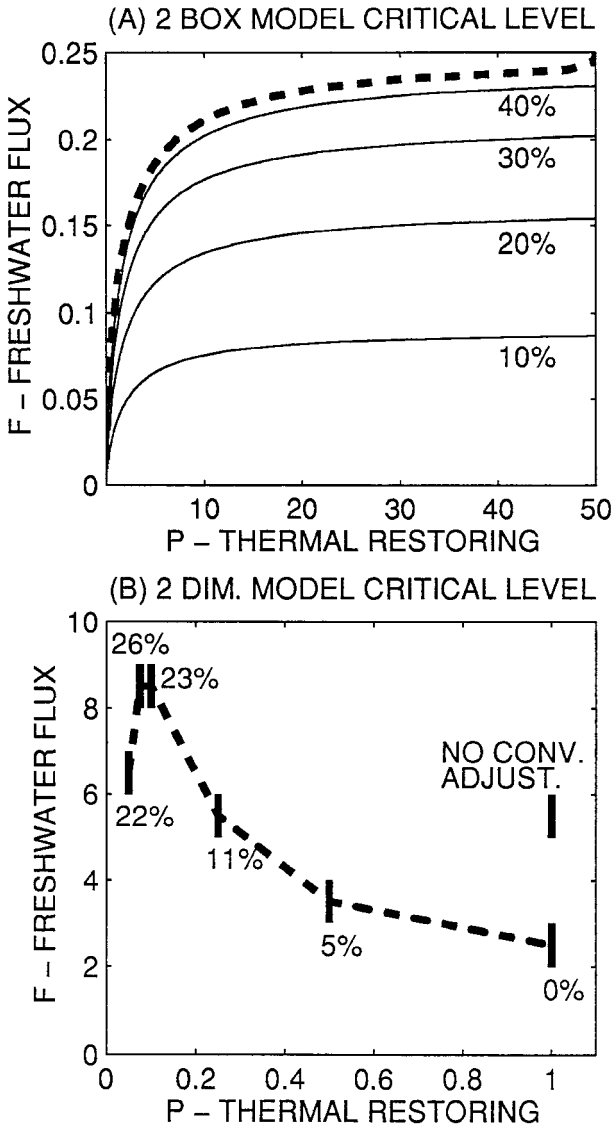

FIG. 1. Critical level of freshening above which there is no steady, thermally direct steady state (thick dashed curve) for a two-box model (a) and a continuous two-dimensional model (b). The contours are the percentage reduction in overturning magnitude relative to an experiment with the same value of P but with $F = 0$. On the bottom panel the vertical lines connect the just subcritical and just supercritical two-dimensional model experiments. Disabling the convective adjustment increased the critical level for a strongly restored case. The percentages refer to the reduction in overturning from an experiment without freshwater forcing to the experiment with just subcritical forcing (the bottoms of the vertical lines). The two models generally have the opposite sensitivity to thermal restoring strength, suggesting that different mechanisms are involved in the breakdown of thermally direct overturning.

relative to internal mixing, thereby further increasing the salinity gradient. The advective instability works by countering the effect of the thermal torque upon the overturning. With stronger thermal restoring, a larger freshwater flux is required to retard the overturning and obtain significant positive feedback from the salt flux boundary condition.

Figure 1b shows the result for the continuous two-dimensional model. Although P in this model is not entirely analogous to P in the two box model since only the surface temperature is directly under its influence, it is rather surprising to see that this model becomes *more* susceptible to freshwater forcing with stronger restoring to the reference temperature profile over most of the range of P. For each value of P, the percentage reduction in overturning magnitude going from the $F = 0$ experiment to the just subcritical experiment has been noted on the figure. In the high P range, where F_{crit} is decreasing with P, the reduction goes to zero. In this region, another kind of instability must be responsible for the breakdown of thermally direct overturning. We will argue that this is a *convective* instability. The distinction between convective and advective processes was first drawn by Bryan (1986) in connection with the timescales of adjustment to fresh and salty perturbations. Zhang et al. (1993) and Rahmstorf and Willebrand (1995) have studied the transient response to impulsive freshening in models with weak and strong thermal damping. They found a reduced response in models with weaker thermal damping. This sensitivity is likely related to the sensitivity of the critical level of the steadily forced model to the strength of the thermal damping.

One piece of evidence that convective instability is responsible for the sensitivity to P comes from applying different values of P over the warm and cold halves of the basin. When this is done, it is found that the critical level of freshwater forcing is not sensitive to the value of P in the warm, ''low-latitude,'' half of the basin. This is consistent with the timescales involved in the problem. In the low-latitude half, heat penetrates diffusively through the thermocline. The timescale for this process is the steady-state basin flushing time by the thermal overturning (Winton 1995b). This is long compared to the timescales of the processes that control the surface, or equivalently, mixed-layer temperature: months for air–sea exchange to several years for the top of the atmosphere radiative balance. Notice that, starting near midbasin, shallow convective layers are found; these deepen moving toward the cold end, finally striking the bottom at the boundary (Fig. 2a). Convection is modeled as an instantaneous process; so in this convecting region, the heat balance *is* affected by the strength of the surface temperature restoring.

Figure 1b also shows the result of a series of experiments performed with a large surface restoring coefficient ($P = 1$) but without convective adjustment. In this case, the cell was able to sustain nearly twice as much freshening as in the convective adjustment case.

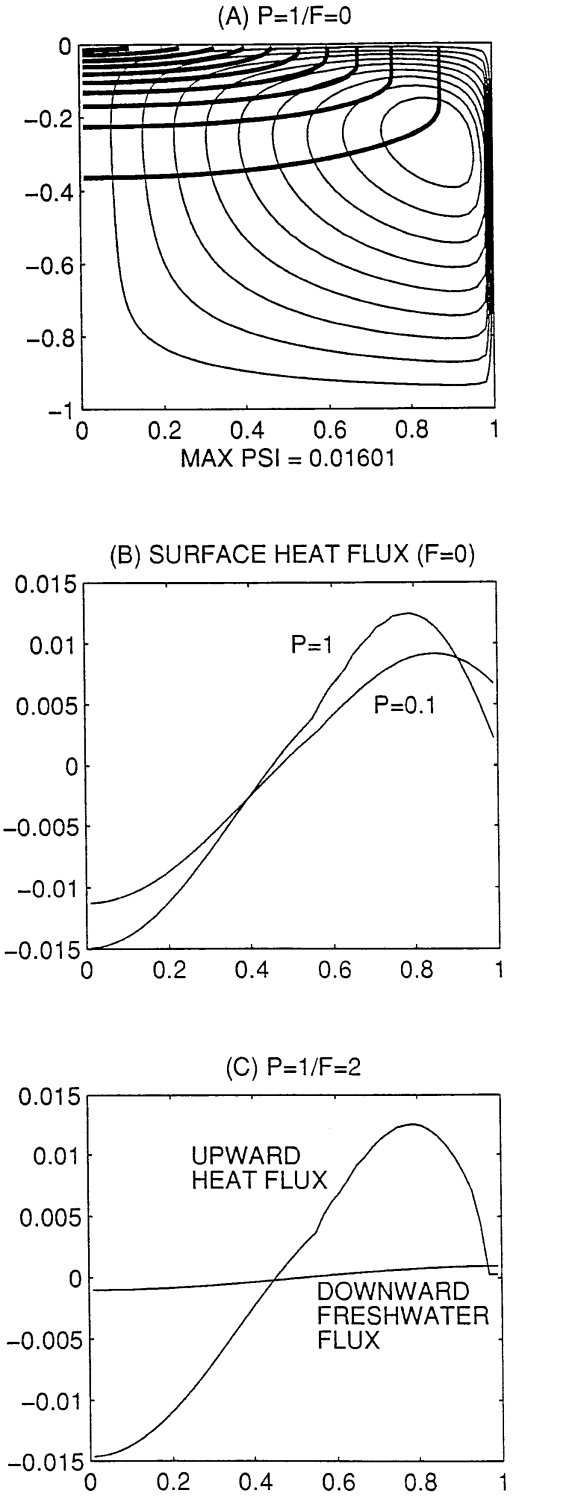

Fig. 2. (a) Two-dimensional model overturning and temperature (thick contours) with strong surface restoring and no freshwater forcing. (b) Comparison of surface heat fluxes for strong and weak thermal restoring with no freshwater forcing. (c) Heat and salt fluxes (in buoyancy units) for the strong thermal restoring case with just subcritical freshwater forcing. The freshening breaks down the circulation by interfering with heat loss rather than by exerting a significant countertorque on the overturning.

This difference in sensitivity is surprising in light of the fact that the deep water is substantially colder in the convective adjustment case and so the no-convection circulation has forgone a substantial portion of the meridional temperature gradient available from the boundary condition. The cold deep water turns out to be exactly the source of instability for the convectively adjusted circulation. Since the deep water has had the benefit of convective cooling, the circulation is ''committed'' to maintaining steady convection. Otherwise, warmer candidate deep water will not sink rapidly and runs the risk of taking on so much fresh water that it may never sink. Thus salinity effects can break down a thermal circulation in two ways: by an adverse meridional torque (advective instability) and by inhibiting high-latitude cooling through stratification (convective instability).

Now let us examine the details behind the sensitivity to P that is evident in Fig. 1b. A rough requirement for local halocline formation is that the downward buoyancy flux due to surface freshening exceeds the upward flux due to surface heat loss (Rahmstorf and Willebrand 1995). This condition is only useful to the extent that heat fluxes are unaltered by the freshening. Note from Fig. 2a that thermal advection is dominantly vertical at low latitude and horizontal at high latitude. Figure 2b shows the upward heat flux with $F = 0$ for steady states with $P = 0.1$ and $P = 1$. In the $P = 1$ case, the temperatures of the convecting layers are effectively pinned at the overlying reference temperatures. Since the reference profile is a half-cosine curve, its meridional derivative goes to zero at $y = 1$ (the ''polar'' boundary). Near $y = 1$, the flow is predominantly meridional, and so the convergence of the heat transport and the surface heat flux go to zero. With the smaller surface restoring coefficient, heat is released through the surface more ''frugally,'' and the water sinks with a temperature above the coldest reference temperature. The excess heat in the deep water may be thought of as left over convective capacity and these considerations highlight the importance of accurately modeling the temperature of the deep water when the issue of thermohaline stability is being addressed.

Figure 2c shows the surface heat flux for the $P = 1$ case with $F = 2$—just below the critical level of freshening. The small amount of freshening is able to dominate the upward heat flux and stratify the water column at the $y = 1$ boundary. With slightly larger freshening ($F = 3$), freshwater pools at the surface and continually interferes with the sinking branch of the circulation to the south. The sinking moves to lower latitudes and shallower depths as the halocline expands. This process has been termed a ''halocline catastrophe.'' The local instability criterion of Rahmstorf and Willebrand that the freshening determine the sign of the surface buoyancy flux is seen to be much too stringent for the global instability that breaks down the overturning cell in the present case. The reason is that freshening influences the heat flux through convection and therefore controls the temperature as well as the salinity of the sinking water.

The extreme sensitivity to freshening described above is associated with the flattening of the reference temperature profile as the $y = 1$ boundary is approached.[1] This might be thought a rather artificial aspect of the forcing. However, it might also be argued that the thermal boundary condition seen by the actual ocean flattens near the poles. We also note that seawater does not go below freezing temperature, but before freezing is reached the buoyancy flux associated with a given heat flux becomes small due to the temperature dependence of the thermal expansion coefficient (the thermal expansion coefficient is small at low temperatures). Beyond the latitude where the water column, or perhaps a substantial portion thereof, is brought to near freezing temperatures, horizontal advection is incapable of supplying a surface thermal buoyancy flux to balance the stratifying effect of a downward freshwater flux and a halocline is formed. Figure 3 depicts a hypothetical scenario for thermohaline instability based upon this effect. The situation at top corresponds to today's warm climate where a substantial portion of the region of net freshening in the North Atlantic (north of roughly 40°N) has temperatures above freezing. Convection in this region mixes down the surface freshening and the bits of halocline that are imported from the north by Ekman drift, gyre circulations, and coastal currents. In the cold climate case below, a larger fraction of the net freshening region has near freezing temperatures and is stratified. Now horizontal mixing of halocline into the convecting region becomes a larger threat to deep water formation.

A particularly tenuous condition might occur when the deep is filled with near freezing water. Since the maximum thermal density of seawater occurs just slightly below freezing, very little upward buoyancy flux can be induced in a column of near freezing water by surface cooling. Consequently the water column is very susceptible to stratification by surface freshening that would cut off the deep water renewal pathway. To the extent that an upward buoyancy flux can be driven by brine ejection from sea ice formation this sensitivity may be averted. In general, sea ice divergence will be necessary to continuously form brine, and continental boundaries may thus constrain the ability of a circulation to maintain itself in this manner.

[1] A reviewer suggested replacing the half-cosine reference temperature profile with linear and stepfunction profiles. With the linear profile, the critical level of the $P = 1$ case is increased from between 2 and 3 to between 8 and 9. With the step profile (step at midbasin), the critical level was larger than 9, as thermal- and haline-direct cells ''peacefully coexisted'' in the warm and cold halves of the basin, respectively. This suggests that both a temperature gradient and a flattening are needed in the net freshening region to produce the sensitivity.

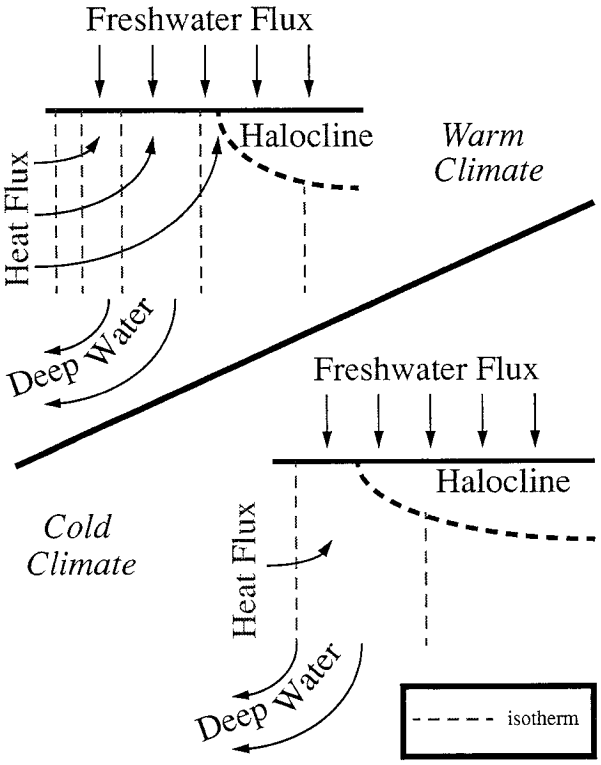

FIG. 3. Cooling-induced convective instability. The schematic represents processes in the high-latitude region of net surface freshening. Surface freshwater mixing between the deep water forming portion and the halocline-covered portion represents a larger threat to steady deep water formation in the *cold* climate case where the latter portion is more extensive due to the reduction in heat available to drive convection.

TABLE 1. Coupled model parameters.

Parameter	Symbol	Value
Rayleigh friction	r	$1.74\cdot10^{-4}$ s^{-1}
Vertical diffusivity	K_v	$5\cdot10^{-5}$ m^2 s^{-2}
Horizontal diffusivity	K_h	10^3 m^2 s^{-2}
Air–sea exchange coefficient	K	40 W °C^{-1} m^{-2}*
Longwave radiation coefficient	B	2.23 W °C^{-1} m^{-2}**
Temperature insensitive part of atmospheric thermal forcing	$A(\phi)$	$A_1(3\sin^2\phi - 1)/2 - B\bar{T}_a$
Amplitude of air temperature gradient forcing	A_1	80 W °C^{-1} m^{-2}
Mean surface air temperature	$\bar{T}_a$	variable

* Loosely based on Haney (1971).
** Based on Oerlemans and Van den Dool (1978).

4. The coupled model

In this section we describe the coupled ocean–atmosphere model that will be used to investigate the sensitivity of NADW formation to climate cooling hypothesized at the end of the last section. Like the model of the last section, the ocean component is two-dimensional in the meridional–vertical plane, with a frictional meridional momentum balance. The equations for the model are

$$0 = -\frac{1}{\rho_0}\frac{\partial P}{\partial y} - rv \tag{5}$$

$$0 = -\frac{1}{\rho_0}\frac{\partial P}{\partial z} - \frac{\rho g}{\rho_0} \tag{6}$$

$$\frac{\partial v}{\partial y} + \frac{\partial w}{\partial z} = 0 \tag{7}$$

$$\frac{\partial T}{\partial t} + v\frac{\partial T}{\partial y} + w\frac{\partial T}{\partial z} = K_h\frac{\partial^2 T}{\partial y^2} + K_v\frac{\partial^2 T}{\partial z^2} + F_T \tag{8}$$

$$\frac{\partial S}{\partial t} + v\frac{\partial S}{\partial y} + w\frac{\partial S}{\partial z} = K_h\frac{\partial^2 S}{\partial y^2} + K_v\frac{\partial^2 S}{\partial z^2} + F_S \tag{9}$$

$$\rho = \rho(T, S), \tag{10}$$

where P is pressure; v and w are the velocities in the meridional and vertical (y and z) directions, respectively; F_T and F_S represent the surface forcings of temperature and salinity; and frictional and diffusive parameters are defined in Table 1. The shorthand $\partial/\partial y \equiv 1/(r_e\cos\phi)(\partial\cos\phi/\partial\phi)$ has been used (ϕ is the latitude and r_e the radius of the earth). This efficient model allows extensive explorations of the parameter space. Another advantage is the ease with which the dynamics of the flow can be understood. A deficiency of the two-dimensional model relative to its rotating, three-dimensional counterpart is that the representation of horizontal (gyre) mode circulations by a horizontal diffusivity does not capture important aspects of the wind-driven circulation [see Winton and Sarachik (1993) for a comparison of similarly formulated two- and three-dimensional models].

The basin is a 60°-wide spherical-coordinate sector from 75°S to 90°N. This domain contains an important oceanographic feature. Above the level of the highest topography in the latitude band of the Drake Passage there is no zonal boundary to support a net geostrophic flow in the meridional direction. This invisible barrier is quite evident in hydrographic properties. In the frictional model, we will represent this by disallowing advective fluxes above 2-km depth between between 54° and 63°S (Fig. 4). Diffusive, convective, and surface fluxes are calculated for this region as in the rest of the domain.

The equation of state used in the model is

$$\rho(T,S) = 0.78S + \begin{cases} 0.129 & \text{if } T < -4.2742°\text{C} \\ -0.0559T - 0.0063T^2 + 3.7315\times10^{-5}T^3 & \text{otherwise.} \end{cases} \tag{11}$$

This form does not allow water below a maximum thermal density temperature of −4.2742°C to become more dense by cooling. Instead of forming sea ice, this model

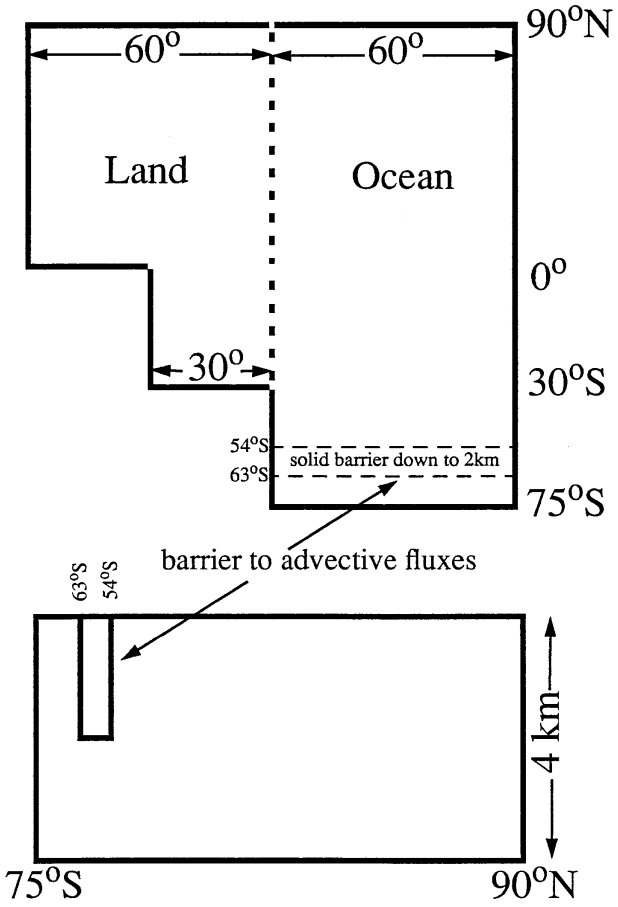

FIG. 4. Coupled model geometry.

forms supercooled water with the maximum thermal density (the maximum density that can be achieved by cooling water of a given salinity). This simplification was made because the two-dimensional ocean model is not expected to adequately model the advection of sea ice. Consequently, the densifying effect of brine rejection is not accounted for by the model.

The model is forced with ''mixed'' boundary conditions, meaning that different forms are chosen for F_S and F_T. Here F_S models evaporation minus precipitation and river runoff as a fixed flux of salinity dependent upon latitude; F_T is chosen as a restoration of the top 50-m grid layer to a reference temperature. It was shown in the last section and has been pointed out previously that the stability characteristics of mixed boundary condition models are dependent upon the strength of this thermal restoring (Zhang et al. 1993; Rahmstorf and Willebrand 1995). Here we implement the restoration of surface temperature by coupling the ocean model to a one-dimensional energy balance atmosphere. In the atmospheric model, the sum of atmospheric heat transport convergence, solar radiation, and a part of the outgoing longwave radiation is a fixed function of latitude. The fixed atmospheric heat transport is consistent with the fixed salt flux boundary condition that implicitly assumes a fixed atmospheric transport of water vapor. Two possible feedbacks are left out by making this simplification: the responses of atmospheric sensible and latent heat transports to changes in SST gradient. We expect that both of these feedbacks will be positive to some degree (Nakamura et al. 1994; Saravanan and McWilliams 1995). A weakening of oceanic overturning and heat transport implies a larger SST gradient and therefore larger atmospheric transports of sensible heat and fresh water. These transports in turn may weaken the driving of the ocean overturning, both by reducing surface density gradients and enhancing the stratification of the high-latitude water column. Since the Atlantic Ocean occupies only a small fraction of Northern Hemisphere latitude bands but responds to atmospheric fluxes over the entire hemisphere (through river runoff and advection of continental air masses), these feedbacks may not be as large as one would expect for an aqua-planet or a planet with periodic replications of continent and deep water forming ocean (e.g., Manabe and Bryan 1985).

The atmospheric model is based upon tracking the energy balance of air parcels as they follow a trajectory over land and sea. It turns out that the strength of the SST damping in such a model is sensitive to the presence of land (Seager et al. 1995; Power et al. 1995). Two processes modify the temperature of the air parcels in our idealized model: radiation and, in the over-sea portion of the trajectory, heat exchange with the surface below. These processes are described by the equation

$$\rho C_p H u \frac{dT_a}{dx} = K(T_s - T_a) - (A + BT_a), \qquad (12)$$

where T_s is the SST, T_a is the atmospheric temperature, and the air–sea exchange coefficient, K, is zero over land. The expression $\rho C_p H u$ represents the advective heat capacity flux of a column of air of height, H, density, ρ, and heat capacity, C_p, per unit mass, traveling at a velocity, u. The linear form $(A + BT_a)$ represents longwave and shortwave radiation and unresolved atmospheric heat transport processes. The latter two are incorporated into A, which is taken to be a function of latitude. As a point of reference let us calculate the heat flux in a trajectory that only passes over water of a uniform temperature (T_s is constant). Term T_a is fixed so (12) is zero and is rearranged to find T_a, giving

$$F = K(T_s - T_a) = \frac{T_s}{\frac{1}{B} + \frac{1}{K}} + \frac{AK}{B + K}. \qquad (13)$$

From this we see that the sensitivity of heat flux to SST will be approximately equal to B since it is roughly 20 times smaller than K ($B \approx 2$ W m^{-2}; $K \approx 40$ W m^{-2}). This important constraint upon thermal damping of surface temperature anomalies was derived in this form by Schopf (1983) and has been used in a thermohaline

circulation model by Zhang et al. (1993). The heat flux–SST sensitivity is closer to B than K because radiation not air–sea exchange represents the limiting constraint upon the flow of heat from the ocean to space—heat ''backs up'' in the atmosphere.

The North Atlantic is notable, however, as a relatively narrow ocean surrounded by land. Since water-mass formation is often associated with the passage of cold, dry continental air masses over the sea, we now investigate the potential enhancement of the heat flux–SST sensitivity in an air trajectory passing over land where no heat is exchanged with the surface. First consider the limiting case of infinitely rapid flow and uniform temperature (a ''well-mixed'' atmosphere) in a trajectory with a land fraction f_l. It is easily shown that, in this case, the heat flux is

$$F = K(T_s - T_a) = \frac{T_s}{\dfrac{1 - f_l}{B} + \dfrac{1}{K}} + \frac{AK}{B + (1 - f_l)K}. \tag{14}$$

Notice that as $f_l \to 1$, the thermal damping goes to K. This is because air–sea exchange will once again become the controling bottleneck as the duration of air parcel exposure to the sea surface becomes short.

To evaluate the accuracy of the well-mixed atmosphere assumption, we solve the complete equation (12). First we solve separately for the temperature over the land and sea portions of the trajectory:

$$T_a = \begin{cases} T_a(x=0)\exp\left(-\dfrac{B}{U}x\right) - \dfrac{A}{B}\left[1 - \exp\left(-\dfrac{B}{U}x\right)\right], \\ \qquad x < f_l \\ T_a(x = f_l)\exp\left[-\dfrac{K+B}{U}(x - f_l)\right] \\ \quad + \dfrac{KT_s - A}{K+B}\left\{1 - \exp\left[-\dfrac{K+B}{U}(x - f_l)\right]\right\}, \\ \qquad x \geq f_l, \end{cases} \tag{15}$$

where $U = \rho C_p Hu/L$, L is the trajectory length, and x ranges from 0 to 1 with land starting at $x = 0$. Solving the system at $x = f_l$ for the temperature as the air column first encounters the sea surface and substituting gives the temperature of the air over the sea:

$$T_a = \frac{KT_s - A}{K + B} - \left(\frac{KT_s - A}{K + B} + \frac{A}{B}\right) \times \frac{\left[1 - \exp\left(-\dfrac{B}{U}f_l\right)\right]\exp\left[-\dfrac{K+B}{U}(x - f_l)\right]}{1 - \exp\left(-\dfrac{B}{U}f_l\right)\exp\left[-\dfrac{K+B}{U}(1 - f_l)\right]}. \tag{16}$$

This expression is averaged over the ocean part of the trajectory and substituted into the expression for surface heat flux to obtain

$$F = K\left\{T_s - \frac{KT_s - A}{K + B} - \left(\frac{KT_s - A}{K + B} + \frac{A}{B}\right)\frac{U}{(K+B)(1 - f_l)} \times \frac{\left[1 - \exp\left(-\dfrac{B}{U}f_l\right)\right]\left(1 - \exp\left[-\dfrac{K+B}{U}(1 - f_l)\right]\right]}{1 - \exp\left(-\dfrac{B}{U}f_l\right)\exp\left[-\dfrac{K+B}{U}(1 - f_l)\right]}\right\}. \tag{17}$$

The third expression in the braces represents the reduction in air temperature over the ocean due to the presence of land. The ratio of this flux to that of the no-land case is plotted in Fig. 5 for $U = 1$ W (m² °C)$^{-1}$ and $U = 4$ W (m² °C)$^{-1}$ along with the same flux ratio

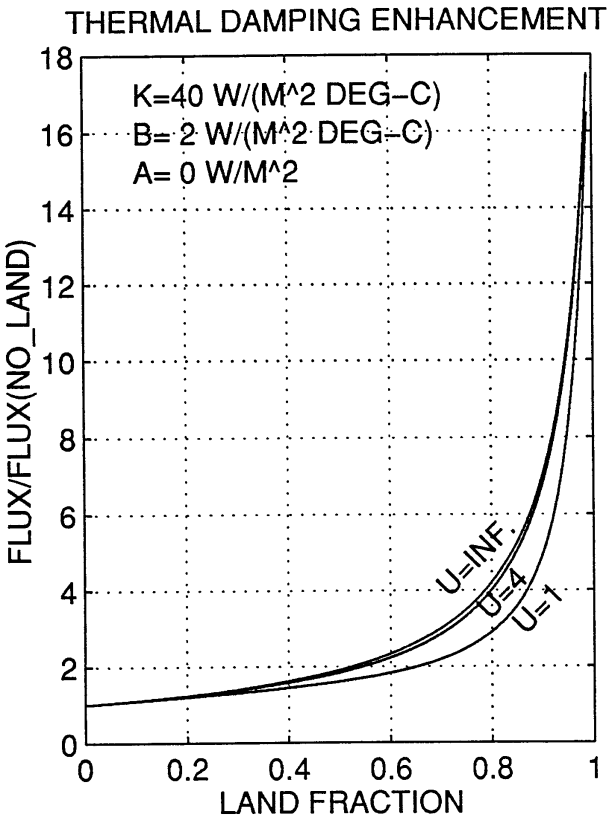

FIG. 5. Enhancement of the thermal damping coefficient due to the presence of a land fraction, f_l, in the air trajectory. The top curve is for a well-mixed atmosphere ($U \to \infty$) case—the ratio of (14) to (13). The bottom curves are for the full solution—the ratio of (17) to (13) with $U = 1$ and 4 W (m² °C)$^{-1}$. For these plots $A = 0$ W m^{-2}, $B = 2$ W (m² °C)$^{-1}$, and $K = 40$ W (m² °C)$^{-1}$.

for the well-mixed atmosphere model. A rough estimate for U using the full heat capacity of the atmosphere traversing a 10 000-km trajectory at 10 m s^{-1} gives, $U \approx 10$ W $(m^2\ °C)^{-1}$. Figure 5 shows that the well-mixed atmosphere assumption is sufficiently accurate to use in the coupled model, so heat fluxes are computed using (14).

As the land fraction increases, Fig. 5 shows that the heat flux–SST sensitivity also increases—air–sea exchange presents a greater bottleneck to the flow of heat from the ocean to space. The bottleneck effect is somewhat larger for larger values of U. For small values of U, the bottleneck presented by mixing of air between land and sea competes with the air–sea exchange bottleneck. Marotzke (1996) contains a related discussion of the impact of atmospheric mixing between land and sea upon thermal damping.

Now we consider the form of A. Since A represents atmospheric heat transport convergence, solar radiation, and the temperature insensitive part of the longwave radiation, it is a function of latitude. We can represent A as the sum of a part that averages to zero over the globe and a constant part as follows:

$$A(\phi) = \frac{A_1(3 \sin^2\phi - 1)}{2 - B\overline{T}_a}, \qquad (18)$$

where A_1 is an amplitude for the forcing of the meridional temperature gradient by atmospheric heat transport convergence and solar radiation and $\overline{T}_a$ is the (specified) global mean air temperature. Term A_1 is chosen to produce realistic SSTs with $\overline{T}_a = 15°C$.

It remains to choose a land fraction for the atmospheric model. Somewhat arbitrarily, this is set to one-half in the Northern Hemisphere, one-third between the equator and 30°S, and 0 south of 30°S (Fig. 4). Other coupled model parameter choices are given in Table 1.

5. Coupled model results

Now we will use the coupled model developed in the last section to investigate changes in NADW formation as the mean atmospheric temperature, $\overline{T}_a$, is varied. The response will be qualitatively different depending upon whether changes in NADW formation can be compensated by changes in Southern Ocean Deep Water. We will explore both cases. The shape-1 (Fig. 6) freshwater forcing curve is relatively symmetric about the equator and will ensure that halocline covers the region south of the circumpolar barrier. The shape-2 forcing allows deep water formation to continue to occur in this region as the magnitude of the freshwater forcing is increased.

The response to cooling under a fixed magnitude of the shape-2 forcing is a continuous replacement of NADW by Southern Ocean Deep Water and a shift to North Atlantic Intermediate Water formation (Fig. 7). Although salinity is not plotted in the figure, the halocline is coextensive with the shallow inverted thermocline next to the northern boundary in each panel. As

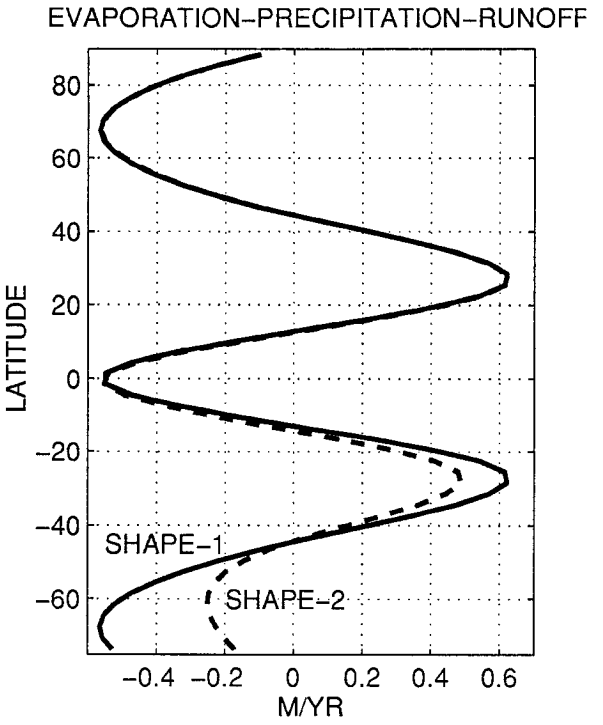

FIG. 6. Reference salt flux boundary condition given as equivalent freshwater flux (35 kg salt ≡ 1 m^3 freshwater). The total freshening of the region north of 40°N is about 0.15 Sv. The shape-2 flux is designed to maintain Southern Ocean Deep Water formation as the magnitude of the fluxes are varied.

the mean atmospheric temperature is cooled from 17° to 15°C, the halocline expands and incorporates the −1°C water that formerly comprised the NADW. The water mass formed just south of the halocline is between 0° and 1°C. Increasing deep ventilation from the south begins to undercut the NADW forming cell. This process continues as the atmospheric temperature is further reduced to 13°C. Now the North Atlantic forms an intermediate water at a temperature between 2° and 3°C just south of an expanded halocline. The overall magnitude of the overturning is only reduced by about 1 Sv from the warmer cases. The principal impact of cooling on northern water mass formation is to allow a spreading of a halocline that interferes with heat loss. The warmer water is not capable of sinking to the bottom so the outflow switches to an intermediate level. A similar shift to intermediate water may be induced by increasing the magnitude of the shape-2 freshwater fluxes under a fixed mean atmospheric temperature. The change in circulation is generally consistent with the altered distribution of deep nutrients inferred from ^{13}C measurements for the last glacial maximum (Duplessy et al. 1988). These measurements indicate a shift in the nutrient-depleted NADW signal from the deep to intermediate levels relative to today's ocean.

The adjustment seen in Fig. 7 involves both advective and convective feedbacks. These interact and so it is

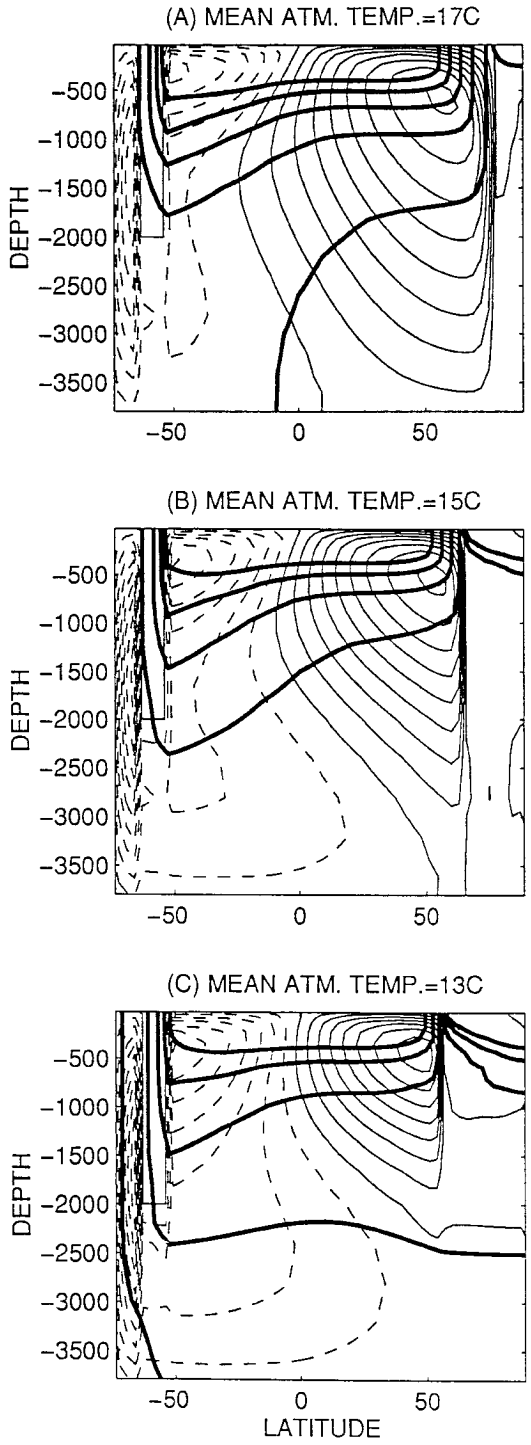

FIG. 7. Circulations under mean atmospheric temperatures of 17°, 15°, and 13°C with 0.6 times the shape-2 fluxes. In the colder climate, the halocline (indicated by the inverted thermocline) spreads, incorporating the colder waters. The warmer sinking waters can only penetrate to intermediate levels, and so in the cold climate, a northern intermediate water replaces the deep water formed in a warm climate. A similar response can be produced by increasing the freshening with a fixed mean atmospheric temperature. Streamfunction contours at 1-Sv intervals (negative dashed); temperature contours (thick solid) at 2°C intervals from −3° to 7°C.

impossible to ascribe the changes in circulation to one or the other alone. However, in view of the fact that 1) the shallowing of the NADW cell is more prominent than its weakening and 2) the decreased density of the sinking water is due to warming that is not an expected consequence of weakened overturning, it seems that convective effects dominate the adjustment process. This is in contrast to the main point made by Manabe and Bryan (1985) in their coupled model study of thermohaline circulations under varying levels of CO_2. They ascribe the relative constancy of overturning in their experiments to the fact that, due to the temperature dependence of the thermal expansion coefficient, the surface density gradient is maintained even as the surface temperature gradient is reduced in the warm climates. In the experiments shown in Fig. 7, the surface density gradient was also relatively unchanged (a small density range decrease was offset by a proportional decrease in the latitudinal extent of the cell) but the circulation changes significantly. Both the effect exhibited in Fig. 7 and the one emphasized by Manabe and Bryan have their source in the nonlinearity of the equation of state. The effect presented here, however, is only expected to come into play at low temperatures.

A point of terminology arises concerning whether or not the behavior exhibited in Fig. 7 should be described as involving an ''instability.'' On one hand the solution seems to adjust smoothly to the change in forcing and there was no hint of multiple equlibria in the spinups to steady state. On the other hand the adjustment is clearly related to the instability that leads to mode flips in the experiments with shape-1 forcing to follow. The evidence for this instability in the Fig. 7 experiments is that the model does not sink water with the maximum thermal density near the edge of its halocline with the position of this edge simply moving equatorward as the cooling progresses. Instead, the halocline overshoots and incorporates increasingly warm water. For this reason, and recognizing that it is a marginal use of the term, we shall refer to the adjustment as involving convective instability.

Now we perform a grid of experiments with a range of mean atmospheric temperatures and magnitudes of the shape-1 freshwater forcing curve (the values plotted in Fig. 6 are simply multiplied by a constant). These experiments reveal a well-defined critical level of freshening (Fig. 8). Below the critical line, the solutions are steady and contain an interhemispheric NADW cell with outflow adjacent to the bottom. Immediately above the line the solutions are self-sustaining deep-decoupling oscillations for $\overline{T}_a$ from 13° to 17°C and steady Southern Ocean Deep Water formation (north of the circumpolar barrier) for the $\overline{T}_a = 18°$ and 19°C cases. The critical level of freshening generally decreases with temperature with a dramatic drop-off between $\overline{T}_a = 17$ and 18°C.

Although the model does not contain a relationship between the mean atmospheric temperature and the strength of the freshwater forcing (the atmospheric wa-

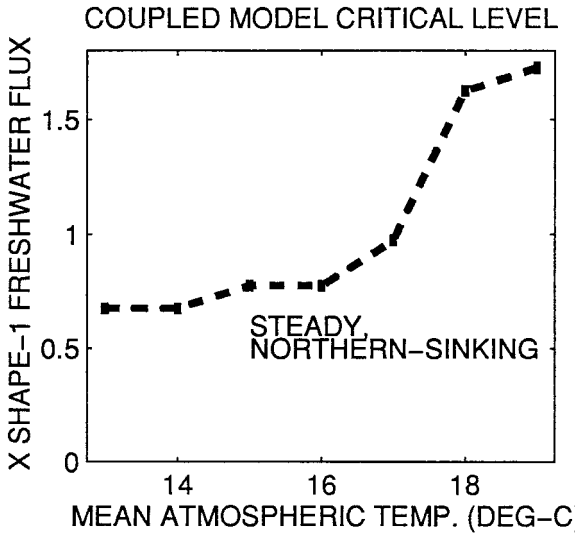

FIG. 8. Variation of critical freshening level with mean atmospheric temperature in the model forced with shape-1 fluxes. The supercritical behavior is oscillatory for mean atmospheric temperatures of 13° through 17°C, and steady Southern Ocean Deep Water formation north of the circumpolar ocean for atmospheric temperatures of 18° and 19°C.

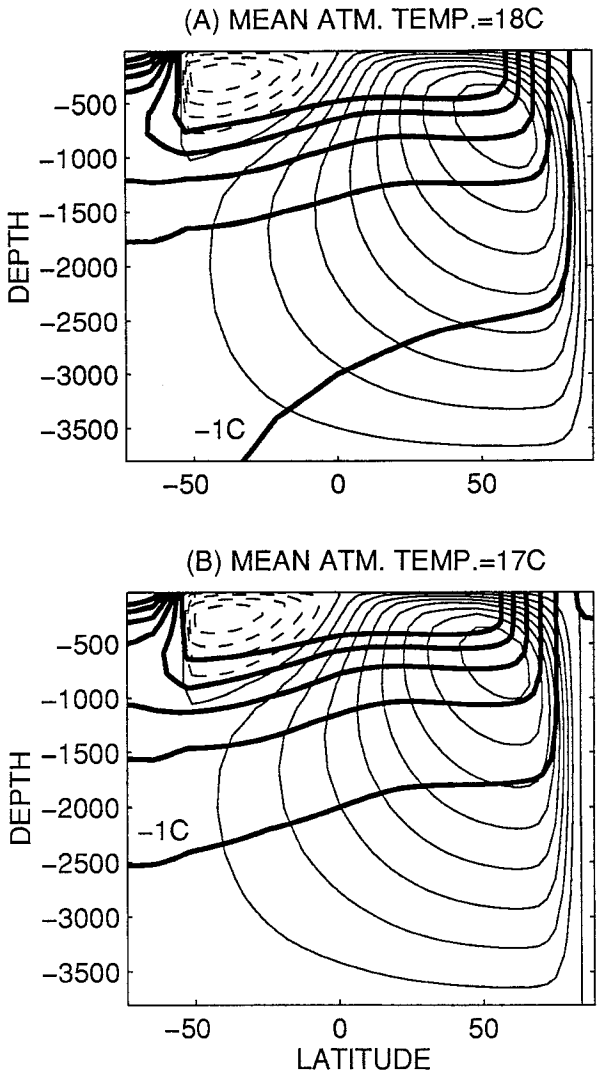

FIG. 9. Circulation under mean atmospheric temperatures of 18° and 17°C with 0.8 times the shape-1 fluxes. As the climate cools toward the critical level, the deep water becomes cooler and a halocline forms in the polar region. With slightly more cooling this halocline prevents the cold water from sinking and self-sustaining deep-decoupling oscillations ensue. Streamfunction contours at 1-Sv intervals (negative dashed); temperature contours (thick solid) at 2°C intervals from −3° to 7°C.

ter vapor transport), we would like to address the issue of compensating changes in the susceptibility of the thermohaline circulation to freshening and the strength of the hydrological cycle as the mean atmospheric temperature changes. We can do this crudely by comparing the slope of the critical level with the variation of saturation vapor pressure with temperature following the Clausius–Clapeyron equation:

$$\frac{d \ln e_s}{dT} = \frac{L}{R_v T^2} \approx \frac{6.5\%}{^\circ\text{C}}, \tag{19}$$

where L is the latent heat of vaporization and R_v is the water vapor gas constant. This gives roughly a doubling of the water vapor holding capacity of air for a 10°C increase in temperature. Figure 8 shows that the critical level of freshening roughly doubles with a 2°C warming from 16° to 18°C. If the freshening were to change in proportion to the saturation vapor pressure of the mean atmospheric temperature, a cooling in this range would induce instability assuming that the overall level of freshening was not too high or too low to cross the instability threshold. This is because the critical level of freshening needed for instability is reduced by cooling more rapidly than the actual level of freshening.

It is of interest to examine the circulation changes that occur as the mean atmospheric temperature is reduced toward the critical level with a fixed level of freshening. Figure 9 shows the solution for a freshening of 0.8 times the shape-1 forcing with $\overline{T}_a = 17°$ and 18°C. A further reduction to $\overline{T}_a = 16.5$°C induced deep-decoupling oscillations so the $\overline{T}_a = 17$°C case is just subcritical. As the onset of convective instability is approached, the overall magnitude of the circulation remains unchanged at 8 Sv. Indeed, the two circulations are different only in two details. The deep water has cooled from −1° to −2°C, and a small bit of halocline appears near the North Pole in the cooler case (indicated by an inverted thermocline). These changes forbode the contradiction the circulation is on verge of encountering—at the same time that the deep water is approaching its maximum thermal density, a halocline is poised to prevent the coldest water from sinking as in Fig. 7.

Figure 10 shows heat flux and temperatures over the self-sustaining deep-decoupling oscillations induced by cooling to $\overline{T}_a = 16$°C. The oscillations can also be in-

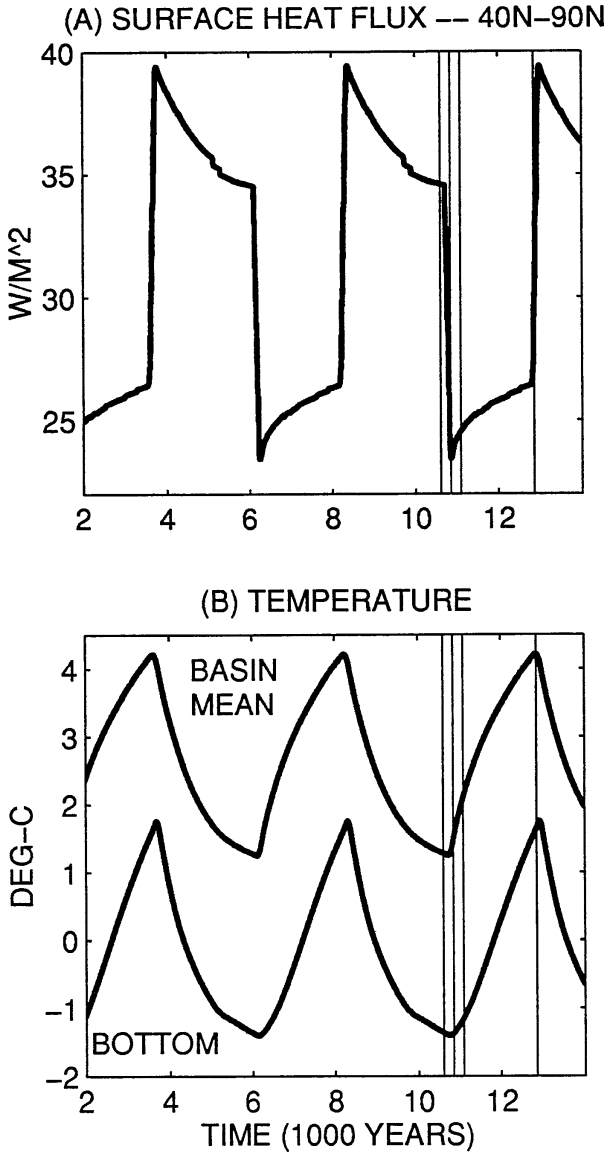

FIG. 10. Variations in high latitude surface heat flux (a) and basin mean and bottom temperatures (b) over deep-decoupling oscillations with a mean atmospheric temperature of 16°C and 0.8 times the shape-1 fluxes.

duced with $\overline{T}_a = 17$°C by increasing the level of freshening. This kind of oscillation, also referred to as *flushes*, has been found in single-hemisphere, two- and three-dimensional models upon switching to mixed boundary conditions (Marotzke 1989; Wright and Stocker 1991; Weaver and Sarachik 1991; Weaver et al. 1993) and by forcing with smooth, large amplitude freshwater patterns (Winton and Sarachik 1993; Winton 1993, 1995a). The oscillations produced here are quite similar to those of Winton (1993). The finding of the oscillations in the present model shows that, although weak thermal damping has been shown to inhibit the polar halocline catastrophe (Zhang et al. 1993; Rahmstorf and Willebrand 1995), rapid convective transitions are still possible. Since the transitions are convective rather than advective, they are fairly well represented by the two-dimensional model. The oscillation exhibits two phases: a deep-coupled phase with deep convection and overturning and a deep-decoupled phase when the deep ocean is not ventilated by advection or convection. The two phases are separated by decadal-scale transitions of the convective state. In the deep-coupled phase, strong poleward heat transport and basin mean cooling lead to large heat fluxes out of the high-latitude ocean (Fig. 10). In the deep-decoupled phase, the opposite situation leads to a reduction in high latitude heat flux as a warm intermediate water cell replaces the deep cell of the deep-coupled phase. Heat transport is reduced partly because the cell is a few Sverdups weaker and partly because the return flow is warmer. Figure 10 shows that the coupled to decoupled transition occurs as the bottom temperature is approaching -2°C.

Figure 11 shows the circulation at the times denoted by the vertical lines in Fig. 10. Figure 11a shows the coldest point in the cycle at the end of the deep-coupled phase. A small halocline is apparent near the northern boundary. In Fig. 11b the circulation is decoupling from the deep ocean as the halocline has spread, engulfing the coldest surface waters. The sinking water is now above 1°C and will not penetrate into the -1°C deep water. Even though the deep water is not directly ventilated it feels the density gradients in the thermocline through the hydrostatic relation. This causes a ''humping up'' of the cold isotherms beneath the intermediate water upwelling. It is the counter pressure gradient due to this effect that evicts the circulation from the deep. Interestingly, the deformation of the deep water also affects the shallow circulation through its impact upon the lid pressure, producing a drag upon the poleward-flowing upper branch. Thus it is more favorable for an overturning circulation to lie adjacent to the bottom than to be separated from it by a layer of ''dead'' water.

Figure 11c shows a point near the beginning of the decoupled phase with significant thermal stratification in the deep. As this phase progresses, the deep water warms through heat diffusion from the overlying intermediate water and this gradient is eliminated. By contrast, the thermocline level thermal structure remains relatively fixed throughout the cycle. Figure 11d shows convection renewing after this has occurred. The basin is much warmer at this point partly because of downward diffusion of heat and partly because of intermediate level ventilation with warmer water. The halocline is completely eliminated at the beginning of the deep-coupled phase, allowing the production of very cold deep water. In the deep-coupled phase, this water sinks vigorously into the warm environment developed over the deep-decoupled phase.

Figure 12 shows the effect of further reducing $\overline{T}_a$ to 15°C. The coupled phases become shorter and the decoupled phases longer. The shortening of the warm

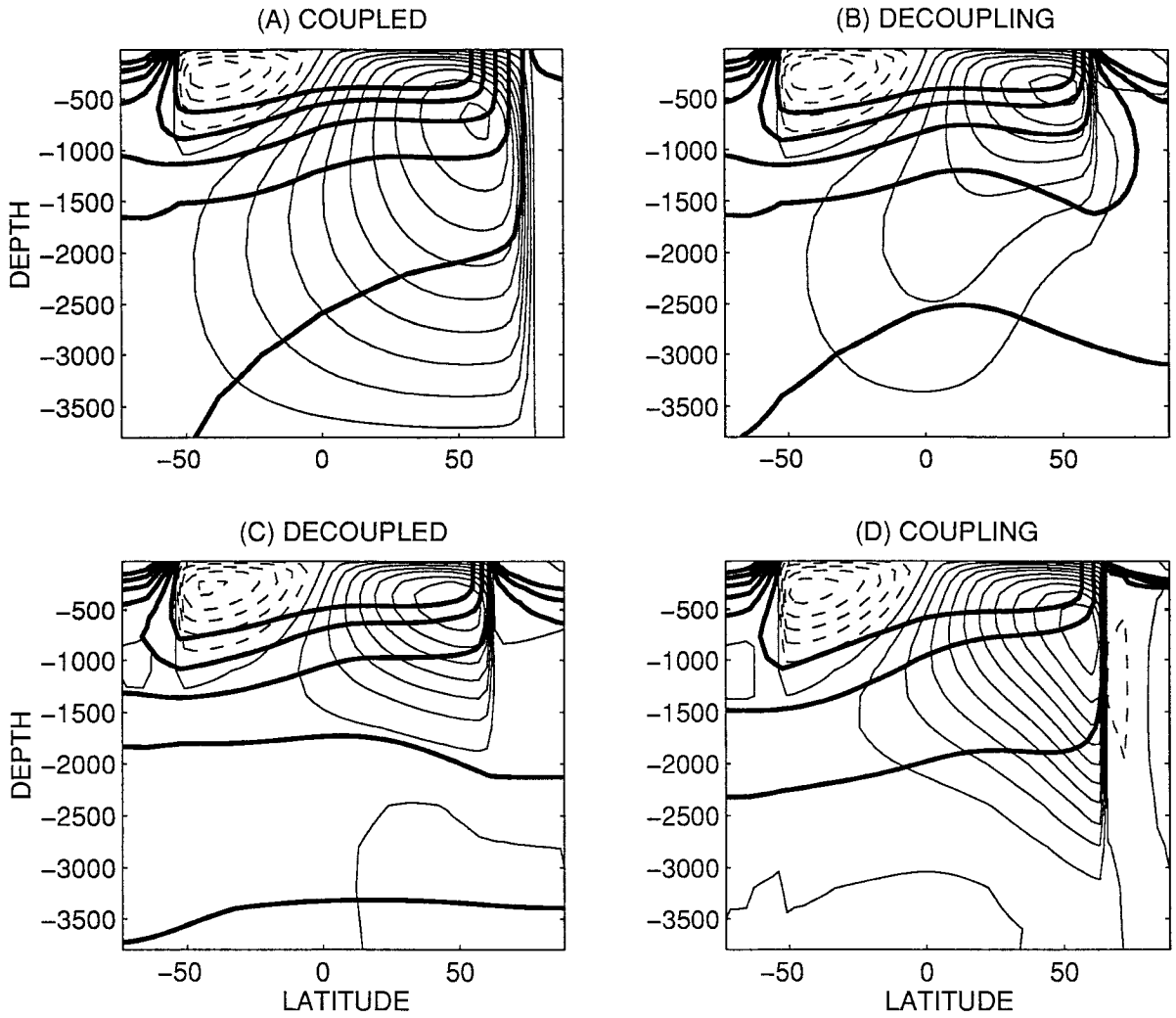

FIG. 11. Snapshots of the circulation at the four times during a deep-decoupling cycle marked by the vertical lines on Fig. 10. Streamfunction contours at 1-Sv intervals (negative dashed); temperature contours (thick solid) at 2°C intervals from −3° to 7°C.

phases is in agreement with the reduction of warm period length in the Dansgaard–Oeschger events during the colder parts of the the glacial cycle. The lengthening of the cold phase, however, does not appear to have a counterpart in the paleo-record. The change in shape with increased freshening (not shown) is qualitatively similar to the change with cooling.

6. Discussion

This paper has focused upon some properties of convective instability that may be useful for understanding differences in North Atlantic Deep Water circulation and stability between glacial and interglacial climates. The convective instability is distinguished from the advective instabilty in that freshening breaks down the circulation by interfering with heat loss rather than by its direct impact upon the salinity of sinking water.

Under the convective instability it was found that increased cooling is generally equivalent to increased freshening. This is so because colder water is less able to maintain convection by an upward thermal buoyancy flux and thus is more susceptible to stratification by the downward buoyancy flux associated with surface freshening. Although a cold climate is in some sense capable of producing more cold water, it is often found that warmer water masses are produced as the colder water becomes bound up in the halocline. This effect leads to a smooth transition from deep water formation to intermediate water formation in the North Atlantic as global cooling progresses in a model that allows compensating ventilation from the south. The change in circulation induced by cooling the model under fixed freshening agrees with ^{13}C evidence for North Atlantic Intermediate Water formation rather than deep water formation during the last glacial maximum.

When Southern Ocean Deep Water formation is suppressed by the pattern of freshening, global cooling un-

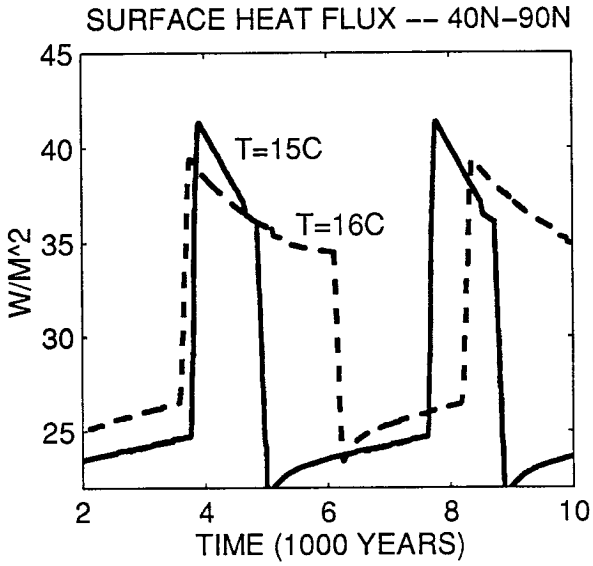

FIG. 12. Variations in high latitude surface heat flux over deep-decoupling oscillations with 0.8 times the shape-1 fluxes and mean of atmospheric temperatures of 16° and 15°C. As the climate cools the warm phases become shorter and the cold phases longer. A similar change can be induced by increased freshening.

der fixed freshening induces deep-decoupling oscillations or Southern Ocean Deep Water formation north of the circumpolar gap in the warmer experiments. The deep-decoupling oscillations are in several respects quite comparable to the Dansgaard–Oeschger events seen in the Greenland ice cores. Like the D–O events there are sharp (decadal) transitions between millennial-scale warm and cold phases. There are also more gradual coolings over the warm phases of the deep-decoupling oscillations, a feature that is also seen in some of the warm interstadial periods of the ice core record. Increased cooling shortens the duration of the deep-decoupling oscillations in agreement with the shorter duration of the interstadials in the colder parts of the glacial era and the 10 000-yr timescale ''Bond Cycles.''

A dramatic decrease in the level of freshening required to breakdown steady NADW formation was found to occur as the deep water temperature approached the maximum in thermal density in the series of experiments where southern ventilation was inhibited. It should be pointed out that the two-dimensional model exhibits a ''cold bias'' in its deep water temperature in contrast to the ''warm bias'' found in many rotating models. It is not clear whether the deep ocean could actually be filled with such cold water and thus encounter such an increased sensitivity to freshening. Some recent evidence from ^{18}O in sediment pore water (Schrag et al. 1996) suggests that at the last glacial maximum, the deep water of the North Atlantic was near freezing, although this water likely originated in the Southern Ocean. The instability described in this paper would be expected to occur only if deep water generated in the north were to reach these low temperatures.

There are two important caveats that should accompany the results of this simple coupled model. The first is that the atmospheric component is not sophisticated enough to account for feedbacks of oceanic heat transport upon atmospheric heat and freshwater transports or even to ensure consistency between the thermal and haline patterns of ocean forcing. We have varied these two independently to examine the sensitivity of the model, but it remains possible, for example, that the overall level of high-latitude freshening in a realistic model would be too low to reveal the effects that have been described in this paper. Only coupled experiments with an atmospheric model that advects heat and water and has realistic diabatic processes will be able to settle this point. Manabe and Bryan (1985) have done such experiments in a simplified geometry. Their lowest CO_2 case shows significant reduction in high-latitude P-E, expansion of sea ice, and weakening of the overturning, but they do not report any time-dependent behavior of their single-hemisphere ocean model.

Second, the two-dimensional ocean model is more likely to produce convective instability than a three-dimensional model. The latter is capable of representing the horizontal segregation of fresh and salty waters. In the subpolar North Atlantic, most of the freshening enters via the boundaries from rivers and the fresh Greenland–Labrador current system (Schmitt et al. 1989). The surface salinity patterns show that much of this freshwater remains confined to the coast in today's ocean. Heat loss from the centers of the convective gyres may thus sustain deep water formation even in the presence of strong freshening. Consistent with this general picture, it has recently been determined that the overturning in a global ocean GCM weakens considerably before shutting down under slowly increased (quasi-steady) freshening (Rahmstorf 1995). This result strongly points to an advective mechanism. Altered patterns of horizontal freshwater transports in the glacial North Atlantic, possibly due to sea ice advection, may therefore be required to induce convective instability.

Acknowledgments. Some early results from this study appeared in Sarachik et al. (1996). The author thanks Stefan Rahmstorf for comments on a draft of that paper. The author is grateful to Tony Broccoli, Steve Griffies, Andrew Weaver, and an anonymous reviewer for helpful reviews of the submitted manuscript of this paper. It is a pleasure to acknowledge interesting discussions with Suki Manabe on the subject matter of the paper. Part of the work was done while the author was a UCAR ocean modeling postdoctoral fellow at the University of Washington.

REFERENCES

Alley, R. B., and Coauthors, 1993: Abrupt increase in Greenland snow accumulation at the end of the Younger Dryas event. *Nature,* **362,** 527–529.

Bond, G., W. Broecker, S. Johnson, J. McManus, L. Labeyrie, J. Jouzel, and G. Bonani, 1993: Correlations between climate records from North Atlantic sediments and Greenland ice. *Nature,* **365,** 143–147.

Boyle, E. A., and L. D. Keigwin, 1987: North Atlantic thermohaline circulation during the past 20,000 years linked to high latitude surface temperature. *Nature,* **330,** 35–40.

Broecker, W. S., 1994: Massive iceberg discharges as triggers for global climate change. *Nature,* **372,** 421–424.

Bryan, F., 1986: High-latitude salinity effects and interhemispheric thermohaline circulations. *Nature,* **323,** 301–304.

Chappellaz, J., T. Blunier, D. Raynaud, J. M. Barnola, J. Schwander, and B. Stauffer, 1993: Synchronous changes in atmospheric CH4 and Greenland climate between 40 and 8 kyr bp. *Nature,* **366,** 443–445.

Dansgaard, W., and Coauthors, 1993: Evidence for general instability of past climate from a 250-kyr ice-core record. *Nature,* **364,** 218–220.

Duplessy, J. C., N. J. Shackleton, R. G. Fairbanks, L. Labeyrie, D. Oppo, and N. Kallel, 1988: Deepwater source variations during the last climatic cycle and their impact on the global deepwater circulation. *Paleoceanogr.,* **3,** 343–360.

Fairbanks, R. G., 1989: A 17,000 year glacio-eustatic sea level record: Influence of glacial melting rates on the Younger Dryas event and deep ocean circulation. *Nature,* **342,** 637–642.

Haney, R. L., 1971: Surface thermal boundary condition for ocean circulation models. *J. Phys. Oceanogr.,* **1,** 241–248.

Keigwin, L. D., W. B. Curry, S. J. Lehman, and S. Johnson, 1994: The role of the deep ocean in North Atlantic climate change between 70 and 130 kyr ago. *Nature,* **371,** 323–326.

Kutzbach, J. E., and H. E. Wright, 1985: Simulation of the climate of 18,000 years bp: Results for the North American/North Atlantic/European sector and comparison with the geologic record of North America. *Quat. Sci. Rev.,* **4,** 147–187.

——, and W. F. Ruddiman, 1993: Model description, external forcing, and surface boundary conditions. *Global Climates Since the Last Glacial Maximum,* H. E. Wright and coeditors, University of Minnesota Press, 12–23.

MacAyeal, D. R., 1993: Binge/purge oscillations of the Laurentide ice sheet as a cause of the North Atlantic Heinrich events. *Paleoceanogr.,* **8,** 775–784.

Manabe, S., and A. J. Broccoli, 1985: The influence of continental ice sheets on the climate of an ice age. *J. Geophys. Res.,* **90,** 2167–2190.

——, and K. Bryan, 1985: CO_2-induced change in a coupled ocean–atmosphere model and its paleoclimatic implications. *J. Geophys. Res.,* **90,** 11 689–11 707.

——, and R. J. Stouffer, 1988: Two stable equilibria of a coupled ocean–atmosphere model. *J. Climate,* **1,** 841–866.

Marotzke, J., 1989: Instabilities and multiple steady states of the thermohaline circulation. *Oceanic Circulation Models: Combining Data and Dynamics,* D. L. T. Anderson and J. Willebrand, Eds., NATO ASI Series, Kluwer, 501–511.

——, 1996: Analysis of thermohaline feedbacks. *Decadal Climate Variability: Dynamics and Predictability,* D. L. T. Anderson and J. Willebrand, Eds., NATO ASI Series. Springer-Verlag, in press.

McManus, J. F., G. C. Bond, W. S. Broecker, S. Johnson, L. Labeyrie, and S. Higgins, 1994: High-resolution climate records from the North Atlantic during the last interglacial. *Nature,* **371,** 326–329.

Nakamura, M., P. H. Stone, and J. Marotzke, 1994: Atmospheric coupling for freshwater and heat fluxes in ocean box models. *J. Climate,* **7,** 1870–1882.

Oerlemans, J., and H. M. Van den Dool, 1978: Energy balance climate models: Stability experiments with a refined albedo and updated coefficients for infrared emission. *J. Atmos. Sci.,* **35,** 371–381.

Power, S., R. Kleeman, R. Coleman, and B. McAvaney, 1995: Modelling the surface heat flux response to long-lived SST anomalies in the North Atlantic. BMRC Research Rep. #48, 21 pp.

Rahmstorf, S., 1995: Bifurcations of the Atlantic thermohaline circulation in response to changes in the hydrological cycle. *Nature,* **378,** 145–149.

——, and J. Willebrand, 1995: The role of temperature feedback in stabilizing the thermohaline circulation. *J. Phys. Oceanogr.,* **25,** 787–805.

Sarachik, E. S., M. Winton, and F. L. Yin, 1996: Mechanisms for decadal-to-centennial climate variability. *Decadal Climate Variability: Dynamics and Predictability,* D. L. T. Anderson and J. Willebrand, Eds., NATO ASI Series. Springer-Verlag, in press.

Saravanan, R., and J. C. McWilliams, 1995: Multiple equilibria, natural variability, and climate transitions in an idealized ocean–atmosphere model. *J. Climate,* **8,** 2296–2323.

Schmitt, R. W., P. S. Bogden, and C. E. Dorman, 1989: Evaporation minus precipitation and density fluxes in the North Atlantic. *J. Phys. Oceanogr.,* **19,** 1208–1221.

Schopf, P. S., 1983: On equatorial waves and El Nino. II: Effects of air–sea thermal coupling. *J. Phys. Oceanogr.,* **13,** 1878–1893.

Schrag, D., G. Hampt, and D. W. Murray, 1996: The temperature and oxygen isotopic composition of the glacial ocean: Evidence from deep sea pore fluids. *Science,* **272,** 1930–1932.

Seager, R., Y. Kushnir, and M. A. Cane, 1995: A note on heat flux boundary conditions for ocean models. *J. Phys. Oceanogr.,* **25,** 3219–3230.

Stommel, H., 1961: Thermohaline convection with two stable regimes of flow. *Tellus,* **13,** 224–230.

Weaver, A. J., and E. S. Sarachik, 1991: The role of mixed boundary conditions in numerical models of the ocean's climate. *J. Phys. Oceanogr.,* **21,** 1470–1493.

——, J. Marotzke, P. F. Cummins, and E. S. Sarachik, 1993: Stability and variability of the thermohaline circulation. *J. Phys. Oceanogr.,* **23,** 39–60.

Winton, M., 1993: Deep decoupling oscillations of the oceanic thermohaline circulation. *Ice in the Climate System,* W. R. Peltier, Ed., NATO ASI Series, Vol. 12, Springer-Verlag, 417–432.

——, 1995a: Energetics of deep-decoupling oscillations. *J. Phys. Oceanogr.,* **25,** 420–427.

——, 1995b: Why is the deep sinking narrow? *J. Phys. Oceanogr.,* **25,** 997–1005.

——, and E. S. Sarachik, 1993: Thermohaline oscillations induced by strong steady salinity forcing of ocean general circulation models. *J. Phys. Oceanogr.,* **23,** 1389–1410.

Wright, D. G., and T. F. Stocker, 1991: A zonally averaged ocean model for the thermohaline circulation. Part I: Model development and flow dynamics. *J. Phys. Oceanogr.,* **21,** 1713–1724.

Zhang, S., R. J. Greatbatch, and C. A. Lin, 1993: A re-examination of the polar halocline catastrophe and implications for coupled ocean–atmosphere models. *J. Phys. Oceanogr.,* **23,** 287–299.